THEORETICA CHIMICA ACTA

Theoret. Chim. Acta (Berl.) 67, 63-89 (1985)

The effect of molecular topology on π-molecular-orbital energies*

Ioan Motoc, Jeremiah N. Silverman, Oskar E. Polansky, and Gottfried Olbrich

Max-Planck-Institut für Strahlenchemie, D-4330 Mülheim a.d. Ruhr, Federal Republic of Germany

Dedicated to Prof. Dr. Günther Wilke on the occasion of his 60th birthday

Three models for constructing topologically related pairs of molecular isomers are discussed at length. The topological-effect-on-molecular-orbitals (TEMO) theorem is presented in detail and illustrated with experimental data; this theorem demonstrates that molecular topology imposes constraints in the form of general interlacing rules on the MO energy patterns of topologically related molecules. Further, non-empirical SCF MO calculations have been performed for topologically related o- and p-divinylbenzenes, difluorobenzenes, benzoquinones, and benzoquinodimethanes in standard and optimized geometries using various basis sets. In most cases, the SCF π-MO eigenvalue patterns of topological related isomers are in complete agreement with the TEMO theorem, thus demonstrating the dominant influence of topology on the π-MO energies. A modified version of the generalized perturbational-variational Rayleigh-Ritz (PV-RR) procedure is described which is used to study the occasional observed deviations from the TEMO predictions; this procedure had been combined with the concept of critical λ (i.e. the threshold value of the perturbation parameter λ at which the TEMO order of a pair of MO eigenvalues starts to invert), thus enabling us to analyze in quantitative detail the physical factors which compete with molecular topology in conditioning the *ab initio* MO energy patterns.

Key words: Topological-effect-on-molecular-orbitals (TEMO) theorem—non-empirical HF SCF calculations—perturbational-variational Rayleigh-Ritz (PV-RR) analysis—topological molecular models

* Part 10 of the TEMO series; for Part 9, see Ref. [9b].

1. Introduction

The constitutional formula of a chemical compound expresses the types of constituent atoms and the pattern of chemical bonds existing among them. Further, the topology of the molecule [1] is delineated by the constitutional formula where the latter is represented by simple graphs. Thus, formally, the molecular topology is fully described by the discrete topological space (i.e. a Hausdorff space) associated with the chemical constitution of the molecule considered [2]. In the case of planar, fully conjugated molecules, the adjacency matrix of the hydrogen-suppressed graph defined in this Hausdorff subspace is isomorphic with the matrix of an effective one-electron Hamiltonian, termed topological, operating on the π-electron functions which neglects all interactions except for the tight-binding ones, where the latter are assumed to be equal for all pairs of atoms; these two matrices differ only in scaling. All of the eigenvalues of this topological Hamiltonian are, of course, simultaneously present as the roots of the associated characteristic poloynomial. Thus, by a global analysis of the relationship between the characteristic polynomials of different chemical systems, one can draw significant conclusions about the topological eigenvalues of the corresponding Hamiltonians.

The goal of this paper is to extend and unify our previous related work [2–7] by (i) discussing in detail the constraints imposed on the eigenvalue spectra by the molecular topology, and by (ii) investigating quantitatively the relationship between the topological and physical factors which compete in conditioning the actual (i.e. *ab initio*) eigenvalue patterns.

Our study is conducted within the framework of non-empirical HF SCF MO calculations augmented in a novel manner by a modified form of the generalized perturbational-variational Rayleigh-Ritz (PV-RR) procedure [8].

To illustrate our procedure, we consider the π-electron MO eigenvalues of several representative planar, topologically related isomers. The separate consideration of π-MO eigenvalues is feasible since the Fock matrix, in its final iterated form, decomposes into σ- and π-blocks. Although we focus our attention on π-MO eigenvalues alone because of their smaller number, it should be noted that the essence of the topological approach is the same for both σ- and π-electrons [2, 3].

In general, one proceeds by comparing the spectra of pairs of molecules which are topologically related in terms of a specified topological model. We say [3] that two molecules are "topologically related" if the topological spaces associated with them may be partitioned into subspaces (corresponding to molecular fragments, or partial structures) which are pairwise isomorphic so that the difference of the two topological spaces arises solely from the neighborhood relations between the subspaces. This implies that topologically related molecules differ only in the connection of pairwise identical partial structures. The general manner in which a pair of topologically related molecules may be constructed is termed a "topological model"; several such models have been described [3, 4, 9]. Further, it has been shown [4] that the topological MO eigenvalues of topologically related

molecules necessarily satisfy a general interlacing theorem termed the topological-effect-on-molecular-orbitals (TEMO) theorem.

The experimental and calculated results presented in this work, as well as previous comparisons with experimental data [3–5] and MO calculations [5–7], satisfy these topologically-founded predictions with astonishing fidelity; this we interpret as evidence for the fundamentality of the linkage between topology and physics presented here. Further, our findings constitute an important justification for the earlier use of topological methods in quantum chemistry [10–13].

This paper is organized as follows: In Sect. 2, the TEMO theorem is presented and illustrated by experimental data for examples of the three topological models treated. Sect. 3 describes our computational methods: In Sect. 3.1, some details of the non-empirical SCF calculations are summarized; in Sect. 3.2. and Appendix A, the generalized PV-RR formalism is modified and combined with refined Rayleigh-Schrödinger (RS) perturbational radii-of-convergence considerations [14] so that it can be effectively applied to the study of TEMO. Sect. 4 presents our computed results. In Sect. 5, these and some additional results are discussed and interpreted, and, finally, in Sect. 6 our conclusions are given.

2. The TEMO theorem

Consider two bivalent partial structures A and B with the inequivalent centers of residual valences denoted by a and b in A, and by c and d in B. A topologically related pair of molecules is formed by suitably connecting A and B with one another: The so-called $\mathcal{S}$ isomer is obtained by linking a with c and b with d, and the $\mathcal{T}$ isomer by linking a with d and b with c.

The characteristic polynomials Φ of the $\mathcal{S}$ and $\mathcal{T}$ isomers in the framework of Hückel theory are given by

$$\begin{aligned}\Phi(\mathcal{S}) = {} & \Phi(A)\Phi(B) - \Phi(A-a)\Phi(B-c) \\ & -\Phi(A-b)\Phi(B-d) + \Phi(A-a-b)\Phi(B-c-d) \\ & -2[\textstyle\sum \Phi(A-P_{ab})][\sum \Phi(B-P_{cd})], \end{aligned} \tag{1}$$

$$\begin{aligned}\Phi(\mathcal{T}) = {} & \Phi(A)\Phi(B) - \Phi(A-a)\Phi(B-d) \\ & -\Phi(A-b)\Phi(B-c) + \Phi(A-a-b)\Phi(B-c-d) \\ & -2[\textstyle\sum \Phi(A-P_{ab})][\sum \Phi(B-P_{cd})], \end{aligned} \tag{2}$$

where $\Phi(A)$, $\Phi(A-a)$, ..., and $\Phi(B-P_{cd})$, respectively, denote the characteristic polynomials of the partial structure A, of the structure obtained from A by removing the vertex a, ..., and of the structure obtained from B by removing the paths P connecting the vertices c and d; in Eqs. (1) and (2), the summation runs over all the respective paths P. The function $\Delta(x)$ defined by

$$\Delta(x) \equiv \Phi(\mathcal{T}) - \Phi(\mathcal{S}), \tag{3}$$

is given in the present case by

$$\Delta(x) = [\Phi(A-a) - \Phi(A-b)][\Phi(B-c) - \Phi(B-d)]; \tag{4}$$

here, x denotes the energy considered as a continuous real variable.

The simplest topological model for constructing $\mathcal{S}$ and $\mathcal{T}$ isomers considers isomorphic partial structures, $A \leftrightarrow B$; this means that A and B may be mapped bijectively onto each other, where the bijections $a \leftrightarrow c$ and $b \leftrightarrow d$ are contained in the mapping. It follows that $\Phi(A-a) = \Phi(B-c)$, $\Phi(A-b) = \Phi(B-d)$, and, hence, (4) takes the form

$$\Delta(x) = [\Phi(A-a) - \Phi(A-b)]^2 \geq 0. \tag{5}$$

Consequently,

$$\Phi(\mathcal{T}) \geq \Phi(\mathcal{S}), \qquad -\infty < x < \infty. \tag{6}$$

This implies [4] that (i) in the closed intervals $[x^{\mathcal{S}}_{2k-1}, x^{\mathcal{S}}_{2k}]$ defined by the eigenvalues $x^{\mathcal{S}}_j$ of $\mathcal{S}$, there are exactly two eigenvalues of $\mathcal{T}$, $x^{\mathcal{T}}_{2k-1}$ and $x^{\mathcal{T}}_{2k}$, and (ii) in the open intervals $(x^{\mathcal{S}}_{2k}, x^{\mathcal{S}}_{2k+1})$, located between the closed ones, there are no eigenvalues of $\mathcal{T}$. The above conclusions can be condensed to the following interlacing rule:

$$x^{\mathcal{S}}_1 \leq x^{\mathcal{T}}_1 \leq x^{\mathcal{T}}_2 \leq x^{\mathcal{S}}_2 \leq \cdots \leq x^{\mathcal{S}}_{2n-1} \leq x^{\mathcal{T}}_{2n-1} \leq x^{\mathcal{T}}_{2n} \leq x^{\mathcal{S}}_{2n}. \tag{7}$$

Table 1. The PE spectra [eV] of tetraphenol ethers, [16]

I[a]		II[a]	
$\mathcal{S}$	$\mathcal{T}$	$\mathcal{S}$	$\mathcal{T}$
	7.82		7.45
8.04		8.02	
8.50		8.51	
	8.69		9.05[b]
	9.80		9.86
9.82		10.46	
10.14			

[a] See Fig. 1 for specification of $\mathcal{S}$ and $\mathcal{T}$ pairs.
[b] Center of a broad band: 8.95–9.14

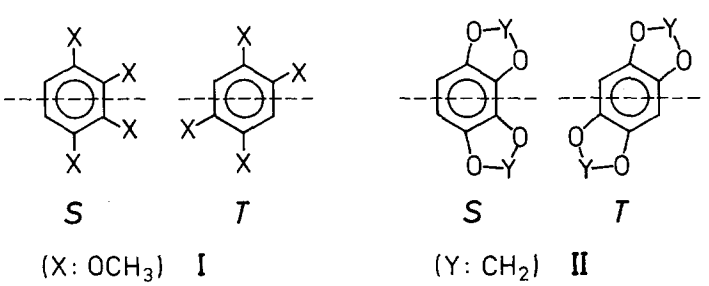

Fig. 1. $\mathcal{S}$ and $\mathcal{T}$ pairs pertaining to model 1

This interlacing rule (7) has been proved rigorously [15] and exhibits the topological-effect-on-molecular-orbitals (TEMO) theorem in its simplest form.

To illustrate the theorem, Table 1 displays the photo-electron (PE) spectra of two $\mathcal{S}$ and $\mathcal{T}$ pairs, namely, the methyl and cyclic methylene ethers, respectively, of tetraphenols (Fig. 1), recently measured in our laboratory [16]. With the assumption of the validity of Koopmans' theorem, the PE spectra reveal the upper part of the energy diagrams of occupied MO's. Hence, comparison of the PE spectra is the most rigorous exmperimental test of TEMO. As seen from Table 1, the TEMO theorem impressively survives this examination.

Another more complex topological model [9] considers three partial structures A, B, and C. Here, A and B are taken to be isomorphic partial structures with the inequivalent centers of residual valence denoted by a and b, attached to the centers u and v, respectively, of the partial structure C. The $\mathcal{S}$ isomer contains the bond sequences $a-u-a$ and $b-v-b$, while $\mathcal{T}$ corresponds to the sequences $a-u-b$ and $b-v-a$. In this case, $\Delta(x)$ takes the form

$$\Delta(x)=\Phi(C-u-v)[\Phi(A-a)-\Phi(A-b)]^2. \tag{8}$$

Evidently, selection of the partial structure C so that $\Phi(C-u-v)\geq 0$ for all x forces satisfaction of $\Delta(x)\geq 0$ in the whole range of x [in analogy with (5)], and the TEMO theorem (7) then holds without restriction. Benzo[c]phenanthrene ($\mathcal{S}$) and chrysene ($\mathcal{T}$) illustrate (Fig. 2) a pair of molecules topologically related by this model.

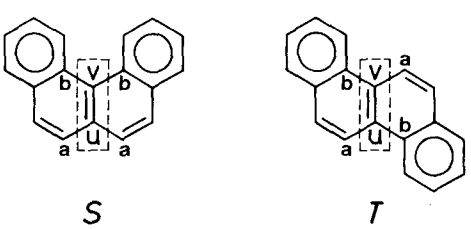

Fig. 2. $\mathcal{S}$ and $\mathcal{T}$ pair pertaining to model 2; the partial structure C is delineated by dotted lines

Table 2. The PE spectra[a] [eV] of benzo[c]phenanthrene ($\mathcal{S}$) and chrysene ($\mathcal{T}$), [17]

$\mathcal{S}$	$\mathcal{T}$
	7.59
7.60	
8.02	
	8.10
	8.68
8.98	
9.18	
	9.43
	9.72
9.96	
10.22	
	10.52

[a] The experimental accuracy is given to ±0.02 eV

The corresponding PE spectra collected in Table 2 are seen to be in excellent agreement with the TEMO theorem (7).

One may construct topologically related molecules in a manner similar to the model leading to (5) and (7), but, in contrast to the latter, the isomorphism of the partial structures is not assumed. Accordingly, $\Delta(x)$ is given in this case by (4). Due to the bilinear form of (4), $\Delta(x)$ need not be non-negative in the whole range of x. It follows that the TEMO theorem (7) now applies in intervals defined by successive real roots of $\Delta(x)=0$, where inversions of the characteristic pattern (7) occur in these successive intervals. The real roots of $\Delta(x)=0$ are termed inversion points and denoted here by x_i^I. Let x_i^I and x_{i+1}^I be two subsequent inversion points, and let $\Delta(x)$ be negative in the interval $x \in (x_i^I, x_{i+1}^I)$. Then, TEMO imposes in this case the following eigenvalue pattern:

$$\begin{aligned} \cdots \leq x_{2k-3}^{\mathscr{S}} \leq x_{2k-3}^{\mathscr{T}} \leq x_{2k-2}^{\mathscr{T}} \leq x_{2k-2}^{\mathscr{S}} \leq x_i^I \\ \leq x_{2k-1}^{\mathscr{T}} \leq x_{2k-1}^{\mathscr{S}} \leq x_{2k}^{\mathscr{S}} \leq x_{2k}^{\mathscr{T}} \leq \cdots \leq x_{i+1}^I \\ \leq x_{2m-1}^{\mathscr{S}} \leq x_{2m-1}^{\mathscr{T}} \leq x_{2m}^{\mathscr{T}} \leq x_{2m}^{\mathscr{S}} \leq \cdots . \end{aligned} \tag{9}$$

This situation is illustrated by the pair of isomers in Fig. 3.

The PE spectra of these compounds are collected in Table 3, and, as anticipated from (4), display two intervals where TEMO inverts the sequence of the MO eigenvalues.

The topological models which satisfy the conditions leading to (5), (8), and (4) are, respectively, termed models 1, 2, and 3. These three models can be further generalized to $\mathscr{S}$ and $\mathscr{T}$ pairs made up of multivalent partial structures. In such cases, Eqs. (4), (5), and (8) correspondingly generalize to more complicated expressions [19] where again $\Delta(x)$ need not be non-negative in the whole range of x. This implies that TEMO then consists of intervals bounded by successive inversion points where inversions of the eigenvalue patterns (7) occur in these intervals, i.e. the molecular topology imposes in these cases the eigenvalue pattern (9).

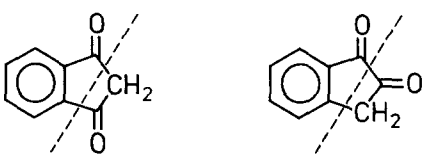

S T

Fig. 3. $\mathscr{S}$ and $\mathscr{T}$ pair pertaining to model 3

Table 3. The PE spectra [eV] of 1,3-($\mathscr{S}$) and 1,2-indandione ($\mathscr{T}$), [18]

$\mathscr{S}$	$\mathscr{T}$
	9.77
9.91	
	9.98
10.15	
10.25	

3. Computational methods for studying TEMO

3.1. Non-empirical SCF MO calculations

The competition between topological and physical factors in conditioning the TEMO pattern can be investigated by performing non-empirical SCF MO calculations for selected pairs of $\mathscr{S}$ and $\mathscr{T}$ isomers; this can be most conveniently accomplished by studying isomers belonging to model 1, where no topologically induced inversions can occur when the moieties A and B are isomorphic and connected by two bonds. This approach is effective because the non-empirical SCF Hamiltonian matrix, in contrast to the topological one, considers all interactions among atoms without any restriction as to their equality. Thus, satisfaction of Eq. (7) argues for the dominance of topological factors while inversions of the TEMO pattern may be traced to the perturbations due to physical factors.

The *ab initio* calculations reported in Sect. 4.1. were performed with the HONDO program [20] using the STO-NG minimal-basis set, $N = 2, 3, \ldots, 6$, [21a]. To supplement this, several other basis sets, i.e. double-zeta [21b], 4-31G [21c], and MINI-4 [21d], have also been employed in calculations of benzoquinones and benzoquinodimethanes; the results of these calculations are reported in Sect. 5.

The SCF MO method is based on the eigenvalue equation,

$$HC = SCE, \tag{10}$$

where H and S are, respectively, the matrix of the HF operator and the overlap matrix, C is the matrix composed of the MO eigenvectors C^s, and E is the diagonal matrix of the corresponding MO energies ε^s, where the superscript s labels the MO.

3.2. Modification of large-order PV-RR *for* TEMO *analysis*

In the event that inversions of the TEMO pattern occur in the non-empirical SCF MO calculations, application of the modified large-order PV-RR analysis presented in this subsection enables us to identify the physical origins of the perturbations on the TEMO patterns and, thus, to dissect in fine detail the relationship between the competing topological and physical factors. As in any *ab initio* calculation, the results may to some extent be an artifact of the basis set used and of their degree of truncation. When we refer to "physical factors", it is with this limitation in mind. Nevertheless, the general method of analysis we introduce in this paper is independent of the degree of approximation arising from the choice of the basis set.

Eq. (10) is the starting point for the application of large-order PV-RR [8]. In the most general PV-RR procedure, all matrices in (10) are treated as functions of a real coupling (perturbing) parameter λ; here λ may either be a natural parameter which varies discretely or continuously over some range of values, thus characterizing a family of solutions, or it may be a dummy ordering parameter whose only physically significant value is unity. In the study of TEMO, λ must be taken

as a dummy parameter [6] where the perturbation is introduced by a model-inspired partitioning [6, 7] of H. For dummy λ, it is both feasible and expedient [8b] to eliminate the S matrix by using the Löwdin [22] symmetric orthonormalization technique. This transformation brings (10) into the canonical form

$$\tilde{H}\tilde{C} = \tilde{C}E; \tag{11a}$$

here, $\tilde{H}$ and $\tilde{C}$ are, respectively, the transformed H and C, and $\tilde{C}$ satisfies the unitary condition

$$\tilde{C}^{\dagger}\tilde{C} = I. \tag{11b}$$

Since the $\mathscr{S}$ and $\mathscr{T}$ isomers of a given pair yield separate and distinct matrix eigenvalue problems, all matrices in (10) and (11) can be appropriately superscripted with $\mathscr{S}$ or $\mathscr{T}$; for brevity, however, we refrain from such superscripting since the meaning will always be clear from the context.

The formally infinite-power series,

$$\tilde{H} = \sum_{j=0}^{\infty} \tilde{H}_j \lambda^j, \tag{12}$$

obtained by partitioning $\tilde{H}$ (as will be subsequently discussed) is taken as known; here, the matrices $\tilde{H}_j$ must be individually Hermitian so that the generalized PV-RR remainder theorem [8b] will apply. In practice, $\tilde{H}$ is partitioned into a finite number of matrices and, hence, the summation of (12) terminates naturally at, say, Jth order. In developing the formalism, however, it is preferable to treat (12) as being of infinite order and then, subsequently, to effect the required reduction for the problem at hand. In any case, the corresponding power series in λ of $\tilde{C}$ and E,

$$\tilde{C} = \sum_{j=0}^{\infty} \tilde{C}_j \lambda^j, \qquad E = \sum_{j=0}^{\infty} E_j \lambda^j, \tag{13a, b}$$

are then computed to *arbitrarily high order* via the PV-RR procedure summarized in Appendix A; here, the $\tilde{C}_j$ are composed of the jth-order MO eigenvector expansion coefficients $\tilde{C}_j^s$ and the E_j are diagonal where the elements ε_j^s are the corresponding jth-order MO eigenvalue expansion coefficients.

We now show how the above formalism can be advantageously modified for the study of TEMO. Since λ is dummy, we are at liberty to partition $\tilde{H}$ for both $\mathscr{S}$ and $\mathscr{T}$ isomers in accordance with topological and/or physical arguments into p well defined steps:

$$\begin{aligned} &\tilde{H}_0 + \tilde{H}_1(1)\lambda = \tilde{H}(1), \\ &\tilde{H}(1) + \tilde{H}_1(2)\lambda = \tilde{H}(2), \\ &\qquad\qquad \vdots \\ &\tilde{H}(p-1) + \tilde{H}_1(p)\lambda = \tilde{H}(p) \equiv \tilde{H}, \end{aligned} \tag{14}$$

where $\tilde{H}_1(q)\lambda$ represents the total perturbation of the qth step.

Here, we select $\tilde{H}_0$ so that it resproduces the TEMO pattern (7) described in Sect. 2. This means that $\tilde{H}_0$ must represent an effective tight-binding Hamiltonian operating in the topological subspace of the π-electron functions in which all diagonal elements are assigned one common value and all non-zero off-diagonal elements are assigned another. In practice, the elements of $\tilde{H}_0$ are constructed by suitably averaging the appropriate elements of the $\mathscr{S}$ and $\mathscr{T}$ HF SCF $\tilde{H}$ as described in detail in Appendix B. Due to the different topological structure of the $\mathscr{S}$ and $\mathscr{T}$ isomers, H_0 evidently also differs for these isomers.

To gain insight into the behavior of the TEMO pattern under perturbations due to various physical $\tilde{H}_1(q)\lambda$, we apply the PV-RR formalism separately to each of the steps (14); criteria for constructing the $\tilde{H}_1(q)\lambda$ are discussed in Sect. 4. Note that this stepwise approach in passing from the TEMO $\tilde{H}_0$ to the SCF $\tilde{H}$ enables us to examine in detail the effect of the successive perturbations on the TEMO pattern. The PV-RR calculations reported in Sect. 4 were performed with a modified version of the computer program [23] which implements the formalism of (12)-(14) and Appendix A; here, as described in Appendix A, one must set the $\tilde{H}_j = 0, j = 2, 3, \ldots$, in the auxiliary matrices defined in Eqs. (A.6) (A.8), and (A.9), in order to reduce the generalized PV-RR formalism to the special case of the linearly perturbed $\tilde{H}(q)$ of (14).

It is clear that the partitioning scheme of (14) will be effective only if the successive perturbations $\tilde{H}_1(q)$, $q = 1, 2, \ldots, p$ are sufficiently small so as to induce convergent PV-RR MO eigenvalue series in each step. The theoretical question of the convergence of RS perturbation series is a difficult one, and, hence, is normally disregarded. In most applications, one merely assumes on the basis of qualitative arguments that the convergence will be rapid if the perturbation is "small" in some imprecisely defined sense. In some cases, however, it is known that apparently small perturbations lead to slowly convergent [14] or strongly divergent [24] RS eigenvalue series. We can deal with this problem quantitatively by using the recently introduced method [14] for obtaining accurate estimates of the radii of convergence of RS perturbation series: The procedure is applicable to the PV-RR expansions of all eigenlevels of *any* linearly perturbed Hamiltonian, e.g., those of (14). In the case at hand, our estimate of the radius of convergence, $r^s(q)$, of the PV-RR series of the sth MO for the qth perturbational step is given in obvious notation [*cf.* (14)] by

$$r^s(q) \approx |\varepsilon_2^s(q)| \{4\tilde{C}_1^{s\dagger}(q)\tilde{C}_1^s(q)[\varepsilon_2^s(q)]^2 + [\varepsilon_3^s(q)]^2\}^{-1/2}, \tag{15}$$

where all the required input data are generated in the first PV-RR cycle. In general, the PV-RR series will converge absolutely for $|\lambda| < r^s(q)$. In the context of TEMO, satisfaction of the condition

$$r^s(q) \gg 1 \tag{16}$$

implies that the associated PV-RR series will converge rapidly. Thus, (15) and (16) provide an independent theoretical criterion for judging perturbational convergence; this supplements the numerical test of summing the PV-RR series to sufficiently high order to reproduce the results of conventional diagonalization.

4. Results

4.1. *Non-empirical* SCF MO *studies*

In this paper, as previously mentioned, we consider the π-MO eigenvalues of a number of representative planar $\mathcal{S}$ and $\mathcal{T}$ isomers; here, the eigenvectors of the σ- and π-MO's are decoupled and we may rigorously treat the latter separately. The non-empirical SCF MO calculations have been performed retaining, respectively, the C_{2v} and D_{2h} (C_{2h} for *p*-divinylbenzene) symmetry of the $\mathcal{S}$ and $\mathcal{T}$ isomers. Further, we have restricted ourselves to isomers which belong to the topological model 1 so that, in the absence of perturbations, the TEMO theorem (7) holds without inversions. Any observed inversions in the TEMO pattern are then studied in Sect. 4.2. via the PV-RR analysis.

Table 4 displays the π-MO energies of the isomers *o*-divinylbenzene ($\mathcal{S}$) and *p*-divinylbenzene ($\mathcal{T}$), as well as *o*-difluorobenzene ($\mathcal{S}$) and *p*-difluorobenzene ($\mathcal{T}$), computed, respectively, in standard and experimentally determined geometries [25] using the STO-3G basis set.

To investigate the influence of the accuracy of the basis set, the π-MO eigenvalues and the total energy E_{total} were computed for the isomers *o*-benzoquinone ($\mathcal{S}$)

Table 4. The π-MO eigenvalues (a.u.) of: (A) *o*-divinylbenzene ($\mathcal{S}$) and *p*-divinylbenzene ($\mathcal{T}$), in standard geometry[a]; (B) *o*-difluorobenzene ($\mathcal{S}$) and *p*-difluorobenzene ($\mathcal{T}$), in experimental geometry[a]

A		B	
$\mathcal{S}$	$\mathcal{T}$	$\mathcal{S}$	$\mathcal{T}$
−0.476015		−0.581785	
	−0.473431		−0.566475
	−0.383621		−0.545391
−0.355225		−0.529275	
−0.353537		−0.434270	
	−0.311884		−0.424011
	−0.279820		−0.301642
−0.257418		−0.289781	
−0.227162		−0.266111	
	−0.220487		−0.258287
	0.203578		0.243637
0.211541		0.247896	
0.240706		0.255351	
	0.266981		0.259370
	0.307425		0.482729
0.360743		0.482836	
0.362925			
	0.402823		
	0.533450		
0.538339			

[a] See [25] for geometrical parameters

Table 5. The π-MO eigenvalues and total energy, E_{total}, in a.u., of *o*-benzoquinone ($\mathscr{S}$) and *p*-benzoquinone ($\mathscr{T}$); STO-*N*G calculations, standard geometry

STO-2G		STO-3G		STO-6G	
$\mathscr{S}$	$\mathscr{T}$	$\mathscr{S}$	$\mathscr{T}$	$\mathscr{S}$	$\mathscr{T}$
−0.509207		−0.535570		−0.538540	
	−0.502984		−0.528679		−0.531682
	−0.432476		−0.462495		−0.466219
−0.391973		−0.423362		−0.427661	
−0.369586		−0.396472		−0.400329	
	−0.319570		−0.346245		−0.350777
	−0.257881		−0.293150		−0.298710
−0.242021		−0.273626		−0.279056	
0.177389		0.136229		0.129836	
	0.179806		0.138212		0.131139
	0.318441		0.278161		0.269349
0.350040		0.303807		0.294638	
0.355484		0.309602		0.300379	
	0.385799		0.333370		0.323759
	0.543760		0.485971		0.474184
0.547740		0.489038		0.477270	
−363.266957[a]	−363.265115[a]	−374.341579[a]	−374.341507[a]	−377.995664[a]	−377.995426[a]

[a] E_{total}

and *p*-benzoquinone ($\mathscr{T}$) using standard geometry [25] and the basis sets STO-*N*G, $N = 2, 3, 6$; these results are presented in Table 5.

The influence of the molecular geometry was then studied by computing the π-MO energies and E_{total} for the same set of $\mathscr{S}$ and $\mathscr{T}$ isomers but now allowing for geometry optimization in the STO-3G basis. The STO-3G optimized geometry was then used in STO-*N*G calculations for $N = 2, 4, 5, 6$. These calculations are systematized in Table 6.

As a further test of the effect of varying N, we have also calculated the gross atom populations of the benzoquinone isomers in optimized geometry for STO-*N*G, $N = 2, 3, \ldots, 6$; the results are collected in Table 7, the atoms being indexed as in Fig. 4.

Finally, Table 8 collects the π-MO energies and E_{total} of the $\mathscr{S}$ and $\mathscr{T}$ benzoquinodimethanes computed in standard geometry for STO-*N*G, $N = 2, 3$, and 6.

It will be noted that the data collected in Tables 4 and 5 are in exact accord with the TEMO theorem (7). In Table 6, however, the pattern is normal for $N = 2$, but for $N \geq 3$, two inversions points, denoted generically by x^I_{Nk}, $k = 1, 2$, appear in the region of virtual orbitals; the position of the x^I_{Nk} is invariant at $x^I_{N1} \approx 0.08$, $x^I_{N2} \approx 0.16$, in the entire range from $N = 3$ to $N = 6$. Further, in Table 8, a single stably located inversion point $x^I_{N1} = -0.4\ldots$ appears in the region of occupied orbitals for all N considered. The physical origin of these inversions is studied in the following subsection.

Table 6. The π-MO eigenvalues and total energy, E_{total}, in a.u., of *o*-benzoquinone ($\mathcal{S}$) and *p*-benzoquinone ($\mathcal{T}$) (STO-*N*G calculations, optimal geometry); x^I_{Ni} denotes the inversion points

STO-2G		STO-3G			STO-4G			STO-5G			STO-6G		
$\mathcal{S}$	$\mathcal{T}$	$\mathcal{S}$	x^I_{3i}	$\mathcal{T}$	$\mathcal{S}$	x^I_{4i}	$\mathcal{T}$	$\mathcal{S}$	x^I_{5i}	$\mathcal{T}$	$\mathcal{S}$	x^I_{6i}	$\mathcal{T}$
−0.493753		−0.521071			−0.523240			−0.523976			−0.524106		
	−0.491948			−0.518547			−0.520645			−0.521395			−0.521530
	−0.426679			−0.457359			−0.460165			−0.460947			−0.461082
−0.392811		−0.424385			−0.427562			−0.428454			−0.428600		
−0.371476		−0.398854			−0.401685			−0.402572			−0.402698		
	−0.324959			−0.351887			−0.355135			−0.356136			−0.356267
	−0.271886			−0.306552			−0.310645			−0.311725			−0.311896
−0.251379		−0.282690			−0.286698			−0.287813			−0.287980		
			0.086970			0.082776			0.080885			0.079799	
0.186900				0.145139			0.139687			0.138420			0.138209
	0.186981	0.145406			0.139956			0.138696			0.138498		
			0.167905			0.162642			0.161657			0.162248	
	0.332891			0.291538			0.284582			0.282927			0.282709
0.353649		0.307220			0.300081			0.298430			0.298181		
0.355024		0.308374			0.301233			0.299576			0.299317		
	0.373768			0.321997			0.314682			0.313044			0.312760
	0.533656			0.476540			0.467427			0.465387			0.465088
0.533950		0.476718			0.467599			0.465568			0.465273		
−363.280637[a]	−363.282544[a]	−374.350257[a]		−374.353250[a]	−377.056434[a]		−377.059421[a]	−377.779826[a]		−377.782763[a]	−378.003781[a]		−378.006716[a]

[a] E_{total}

Table 7. Benzoquinones: Gross atomic populations with STO-NG, $2 \leq N \leq 6$; optimal geometry

Atom		STO-2G	STO-3G	STO-4G	STO-5G	STO-6G
1[a]	1	8.1276	8.1888	8.1982	8.1993	8.1991
	2	5.8678	5.8329	5.8247	5.8233	5.8234
	3	6.0570	6.0804	6.0827	6.0815	6.0813
	4	6.0251	6.0525	6.0533	6.0518	6.0516
	5	0.9606	0.9209	6.9185	0.9201	0.9203
	6	0.9618	0.9245	0.9225	0.9241	0.9243
2[a]	1	8.1364	8.2024	8.2123	8.2133	8.2131
	2	5.8427	5.8141	5.8050	5.8032	5.8035
	3	6.0507	6.0725	6.0746	6.0734	6.0732
	4	0.9597	0.9193	0.9168	0.9183	0.9185

[a] See Fig. 4 for indexing of atoms in the two molecules

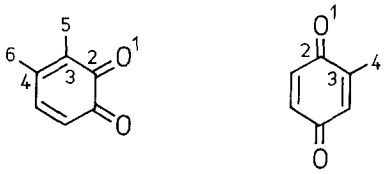

1 2

Fig. 4. The numbering of the atoms in *o*- and *p*-benzoquinone

Table 8. The π-MO eigenvalues and total energy, E_{total}, in a.u., of *o*-benzoquinodimethane ($\mathcal{S}$) and *p*-benzoquinodimethane ($\mathcal{T}$); STO-NG calculations, standard geometry; x^I_{Ni} denotes the inversion points

STO-2G			STO-3G			STO-6G		
$\mathcal{S}$	x^I_{2i}	$\mathcal{T}$	$\mathcal{S}$	x^I_{3i}	$\mathcal{T}$	$\mathcal{S}$	x^I_{6i}	$\mathcal{T}$
		−0.449086			−0.463564			−0.464692
−0.448898			−0.462872			−0.464414		
	−0.447497			−0.444017			−0.462356	
		−0.344181			−0.356040			−0.362163
−0.322789			−0.339028			−0.341584		
−0.318015			−0.334344			−0.337100		
		−0.305918			−.317533			−0.325560
		−0.198066			−0.203487			−0.221607
−0.183816			−0.203380			−0.207698		
−0.201354			0.176918			0.171431		
		0.213662			0.182181			0.183681
		0.346932			0.305279			0.308887
0.364117			0.332594			0.324815		
0.372129			0.340478			0.332432		
		0.400141			0.364449			0.358151
		0.559846			0.514629			0.505754
0.562356			0.518629			0.508081		
−294.856870[b]		−294.870558[b]	−303.774030[b]		−303.780069[b]	−306.762095[b]		−306.775572[b]

[a] Inversion points

[b] E_{total}.

4.2. PV-RR *studies of* TEMO *inversions*

To reconstitute the "history" of TEMO inversions, we have found it advantageous [6, 7] to specialize (14) to the case of $p = 2$ steps as follows: In the first perturbational step, we take

$$\tilde{H}(1) = \tilde{H}_0 + \tilde{H}_1(1)\lambda, \tag{17}$$

where $\tilde{H}_0$ has been previously defined in Sect. 3.2. and $\tilde{H}_1(1)\lambda$ introduces the actual SCF tight-binding interactions[1,2]; then the second perturbational step is given by

$$\tilde{H}(2) = \tilde{H}(1) + \tilde{H}_1(2)\lambda \equiv \tilde{H}, \tag{18}$$

where $\tilde{H}(1)$, (17), is now used as the zero-order Hamiltonian matrix and $\tilde{H}_1(2)\lambda$ accounts for the non-nearest-neighbor interactions.[2] Full details of the construction of $\tilde{H}_1(1)$ and $\tilde{H}_1(2)$ are given in Appendix B. As previously mentioned, due to the different structure of the $\mathscr{S}$ and $\mathscr{T}$ isomers, there is a different set of matrices in (17) and (18) for each of these isomers. We may summarize the content of (17) and (18) by noting that $\tilde{H}_0$ introduces the topological constraint which leads to TEMO, and $\tilde{H}_1(1)$ and $\tilde{H}_1(2)$ introduce the physical factors (i.e. chemical nature and geometrical location of the atoms, and non-nearest-neighbor interactions, respectively) which compete in conditioning the SCF MO eigenvalue pattern.

The PV-RR procedure in conjunction with (17) and (18) was applied to the benzoquinone and benzoquinodimethane isomers using, respectively, the data corresponding to Tables 6 and 8 as input. In all cases, the perturbational convergence of the PV-RR π-MO eigenvalue series was rapid and the calculations were carried out to sufficiently high order to reproduce the results of conventional numerical diagonalization to full accuracy (*e.g.*, for the STO-6G benzoquinone data, the PV-RR series through 5th and 13th order yielded, respectively, an accuracy of 10^{-6} and 10^{-10}). The convergence of these series was also verified independently by computing their radii of convergence $r^s(q)$ via (15).

For the benzoquinone isomers with STO-6G data as input, the PV-RR π-MO eigenvalue series obtained for the first perturbational step, (17), conform completely to the TEMO theorem (7), i.e. generate no TEMO inversions in any order and, hence, are not presented explicitly. The PV-RR π-MO eigenvalue series for the *second* perturbational step, (18), summed through nth order, $n = 0, 1, \ldots, 5$, are collected in Table 9; it should be noted that the sum of the (effectively) infinite-order series resulting from the first perturbational step, (17), coincides

[1] Due to the SCF procedure used to compute the HF MO energies, Eq. (10), the H elements corresponding to the tight-binding interactions contain some contribution from non-nearest-neighbor interactions; we estimate, however, the weight of this contribution to be marginal.

[2] In the present work, we have verified by comparison of H and $\tilde{H}$ that for π-electrons, the orthonormalization procedures of [22] only slightly modifies the original basis set in transforming (10) to (11a).

with the unperturbed ($n = 0$) MO eigenvalue entries for the second perturbational step, (18).

It is seen from Table 9 that the two SCF inversion points x_{61}^I and x_{62}^I of Table 6 do indeed appear in this second step. In Table 10, the influence of the basis

Table 9. Benzoquinones: Summation of π-MO PV-RR eigenvalue series in a.u., through nth order of second perturbational step (optimal geometry, STO-6G input); x_i^I denotes the inversion points

$n=0$		$n=1$			$n=2$		
$\mathscr{S}$	$\mathscr{T}$	$\mathscr{S}$	x_i^I	$\mathscr{T}$	$\mathscr{S}$	x_i^I	$\mathscr{T}$
−0.557362		−0.523454			−0.524046		
	−0.553500			−0.520983			−0.521507
	−0.462062			−0.461052			−0.461082
−0.422020		−0.427944			−0.428499		
−0.400092		−0.402817			−0.402739		
	−0.350053			−0.356267			−0.356267
	−0.270827			−0.311683			−0.311921
−0.247823		−0.288253			−0.288100		
			0.088289			0.079853	
0.132057				0.138179			0.138209
	0.133278	0.138367			0.138493		
			0.156840			0.161875	
	0.290404			0.282709			0.282709
0.299363		0.297780			0.298167		
0.300273		0.299012			0.299331		
	0.307919			0.312000			0.312762
	0.452832			0.465087			0.465088
0.453489		0.465194			0.465277		

$n=3$			$n=4$			$n=5$		
$\mathscr{S}$	x_i^I	$\mathscr{T}$	$\mathscr{S}$	x_i^I	$\mathscr{T}$	$\mathscr{S}$	x_i^I	$\mathscr{T}$
−0.524097			−0.524104			−0.524106		
		−0.521528			−0.521530			−0.521530
		−0.461082			−0.461082			−0.461082
−0.428581			−0.428597			−0.428600		
−0.402707			−0.402700			−0.402698		
		−0.356267			−0.356267			−0.356267
		−0.311897			−0.311897			−0.311896
−0.288997			−0.287983			−0.287980		
	0.080198			0.079886			0.079799	
		0.138209			0.138209			0.138209
0.138493			0.138498			0.138498		
	0.161941			0.162207			0.162248	
		0.282709			0.282709			0.282709
0.298181			0.298181			0.298181		
0.299316			0.299317			0.299317		
		0.312759			0.312761			0.312760
		0.465088			0.465088			0.465088
0.465272			0.465273			0.465273		

Table 10. Benzoquinones, optimal geometry: The influence of basis set on radii of convergence of second perturbational step

$r^s(2)$	$\mathscr{S}$ isomer STO-2G	STO-3G	STO-6G	$\mathscr{T}$ isomer STO-2G	STO-3G	STO-6G
$r^1(2)$	8.2	8.3	8.4	14.1	14.8	14.9
$r^2(2)$	5.3	5.5	5.5	60.8	61.4	64.0
$r^3(2)$	2.3	2.5	2.4	∞	∞	∞
$r^4(2)$	1.8	1.6	1.5	7.4	8.6	8.8
$r^5(2)$	20.5	22.7	22.4	60.7	61.6	64.2
$r^6(2)$	16.8	17.4	17.6	∞	∞	∞
$r^7(2)$	13.7	12.3	12.2	16.5	15.5	15.4
$r^8(2)$	9.2	13.6	13.9	27.6	96.1	73.7

set on the convergence properties of the PV-RR π-MO eigenvalues is investigated by collecting the $r^s(2)$ for the benzoquinone isomers in optimized geometry computed with STO-NG, $N=2, 3$, and 6.

Finally, for the benzoquinodimethane isomers with STO-3G data as input, the PV-RR π-MO eigenvalue series for the *second* perturbational step, summed through nth order, $n=0, 1, \ldots, 4$, are presented in Table 11; the corresponding $r^s(2)$ are also tabulated. It will be noted from Table 11 that the SCF inversion point x'_{31} of Table 8 is generated during this second perturbational step; as in the case of the benzoquinone isomer, TEMO inversions do not appear in the first perturbational step, and the corresponding PV-RR π-MO eigenvalue series summed through infinite order are entered under the $n=0$ heading.

5. Discussion

We can gain insight into the interplay between molecular topology and physics by discussing and interpreting the various interesting features which emerge from a study of the non-empirical SCF and PV-RR results in Tables 4–11.

(i) It is seen from Table 4 that the MO eigenvalue patterns for the divinylbenzene and difluorobenzene isomers obey the TEMO theorem (7) in, respectively, standard and experimental geometries. Evidently, for these isomers, physically induced perturbations are negligible and the topological constraints (5) imposed by model 1 predominate.

(ii) Tables 5 and 6 show, however, that the situation is quite different for the benzoquinone isomers. Thus, in standard geometry (Table 5) no inversion occurs and, further, this result is independent of the basis set considered. We conclude that topology predominates in standard geometry. On the other hand, in optimized geometry (Table 6), as previously mentioned, the TEMO pattern obeys (7) only for $N=2$, but two stably located inversion points appear in the range $3 \leq N \leq 6$. We interpret these findings by noting that in optimized geometry the surroundings of each atom in the two molecules are less similar than in the case of standard geometry; in addition, the physical factors are not held constant in passing from

Table 11. Benzoquinodimethanes: Summation of π-MO PV-RR eigenvalue series, in a.u., through nth order of second perturbational step (standard geometry, STO-3G input)[d]

	$n=0$		$n=1$			$n=2$			$n=3$			$n=4$		
$r^x(2)$	$\mathscr{S}$	$\mathscr{T}$	$\mathscr{S}$	x_i^{Ic}	$\mathscr{T}$	$\mathscr{S}$	x_i^{Ic}	$\mathscr{T}$	$\mathscr{S}$	x_i^{Ic}	$\mathscr{T}$	$\mathscr{S}$	x_i^{Ic}	$\mathscr{T}$
17.1[a]	−0.497043				−0.463215			−0.463541			−0.463561			−0.463564
13.4[b]		−0.495944	−0.462545			−0.462858			−0.462871			−0.462872		
				−0.444130			−0.444244			−0.444054			−0.444017	
14.1[a]		−0.350148			−0.355588			−0.356059			−0.356039			−0.356040
16.6[a]	−0.332674		−0.338773			−0.339038			−0.339028			−0.339028		
23.3[a]	−0.326557		−0.334076			−0.334343			−0.334344			−0.334344		
∞[b]		−0.308439			−0.317533			−0.317533			−0.317533			−0.317533
2.7[b]		−0.165294			−0.203459			−0.203506			−0.203489			−0.203487
7.5[a]	−0.161900		−0.203293			−0.203393			−0.203380			−0.203380		
18.7[a]	0.162444		0.176560			0.176922			0.176917			0.176918		
8.8[b]		0.164592			0.181948			0.182206			0.182181			0.182181
∞[b]		0.311820			0.305279			0.305279			0.305279			0.305279
21.0[a]	0.334629		0.332369			0.332586			0.332593			0.332594		
20.5[a]	0.340315		0.340250			0.340484			0.340477			0.340478		
22.1[b]		0.362375			0.364071			0.364445			0.364448			0.364449
22.0[b]		0.506953			0.514412			0.514624			0.514629			0.514629
18.4[a]	0.509779		0.518501			0.518635			0.518629			0.518629		

[a] The $\mathscr{S}$ isomer.
[b] The $\mathscr{T}$ isomer.
[c] Inversion points.
[d] For $n=4$ and $n=11$, all series have respectively converged to an accuracy of 10^{-6} and 10^{-10}.

$\mathcal{S}$ to $\mathcal{T}$ and compete with topology in determining the eigenvalue spectrum; moreover, the non-equality of various interactions (i.e. among nearest- and non-nearest-neighbors) is accentuated by the incongruence of the geometries of partial structures in the geometrically optimized $\mathcal{S}$ and $\mathcal{T}$ isomers. All of these factors argue that, in general, physically induced perturbations become more significant in optimized geometry. The failure of TEMO inversions to occur for the STO-2G calculations in optimized geometry may be attributed to the reduced accuracy of this basis [21a]. This is in parallel trend with the values of E_{total} in Table 6 where there is a large gap between the poor results obtained for $N=2$ and the considerably improved, closely bunched results for $N \geq 3$; further evidence of this effect is furnished by the gross atom populations presented in Table 7 where it is seen that the STO-2G calculations indicate significantly less polarized electronic structures as compared with the STO-NG, $3 \leq N \leq 6$.

From this, and the stable TEMO inversion pattern for $3 \leq N \leq 6$, it is tempting to conjecture qualitatively that the TEMO pattern (7) represents the limiting behavior on passing from accurate (physically oriented) to less accurate (topologically oriented) basis sets.

(iii) Disregarding for the moment the question whether the inversions depend upon the choice of the basis set, we now investigate the origins of the TEMO inversions using the example of benzoquinone isomers displayed in Table 6. This is done by means of the PV–RR analysis of the STO-6G data presented in Table 9. As previously mentioned, inspection of Table 9 reveals that the first perturbational step has no effect on the TEMO pattern (7), but the second perturbational step does indeed generate the two SCF inversion points x_{61}^I and x_{62}^I in the range of virtual orbitals (cf. Table 6). Moreover, the location of these inversion points is already correctly and stably established by the *first-order* perturbational correction ($n=1$) of (18) to the eigenvalues of $\tilde{H}(1)$; higher-order perturbational corrections in (18) merely bring about greater numerical accuracy in the values of the x_{6k}^I but do not change the associated pattern. The standard physical intepretation of the first-order perturbation energy then leads to the following conclusion: The TEMO inversions exhibited in the STO-6G representation by the $\mathcal{S}$ and $\mathcal{T}$ benzoquinone π-MO eigenvalue spectra are due to the averaged effect of the significant and possibly non-equal non-nearest-neighbor interactions. Further, our results also clearly prove that the perturbing influence of the actual SCF nearest-neighbor interaction on the TEMO pattern is negligible in this case. In addition, as may be seen from the data in Table 10, the perturbational convergence of all PV–RR series to the proper limit is assured since in the majority of cases, the very strong condition (16) is fulfilled, while in the few remaining cases, $r^s(q) > 1$ by a comfortable margin; in this context, it is interesting to note that increasing the accuracy of the STO-NG basis set by varying N has only a negligible effect on the convergence properties of the series. Thus, we have proved that, in the framework of the minimal STO-NG basis set, the *ab initio* calculations for the benzoquinone isomers in optimized geometry simulate the variant of topological model 1 where A and B are isomorphic but multivalent partial structures. These results are in accord with our earlier conclusions [7] based only

on STO-NG data. The very small energy difference (about 0.0003 a.u.) between the (LUMO) orbitals of the $\mathcal{S}$ and $\mathcal{T}$ isomers raises the possibility that the TEMO inversions located at $x_1^I \simeq 0.08$ and $x_2^I \simeq 0.16$ a.u. (Table 6) may be due to the choice of the STO-NG basis set. This possibility prompted us to repeat these calculations employing the more flexible 4-31G [21c] and double-zeta [21b] basis sets; it is seen from these results, which are presented in Table 12, that no TEMO inversions occur.

Thus, the comparison of Table 6 and 12 suggests that the two inversion points observed in STO-NG calculations are actually due to the insufficient flexibility of this basis; we return to this point later in this section.

(iv) Now consider the PV-RR analysis of the STO-3G data for the $\mathcal{S}$ and $\mathcal{T}$ isomers of the benzoquinodimethanes presented in Table 11. The results of Tables 8 and 11 for the benzoquinodimethane isomers are, respectively, qualitatively similar to those of Tables 6 and 9 for the benzoquinone isomers except that for the former isomers only a single inversion point x_{31}^I appears, located this time in the range of occupied orbitals. Once again, the first perturbational step has no influence on the TEMO pattern (7), while the first-order perturbational correction of the second perturbational step correctly and stably generates the SCF location of this single inversion point. By exactly the same arguments, it follows that the TEMO inversion in the case of the benzoquinodimethanes is also due exclusively to the averaged effect of the significant and possibly non-equal non-nearest-neighbor interactions. Finally, inspection of the $r^s(2)$ collected in

Table 12. The π-MO eigenvalues and total energy, E_{total}, in a.u., of *o*-benzoquinone ($\mathcal{S}$) and *p*-benzoquinone ($\mathcal{T}$)

4-31G		Double-zeta	
$\mathcal{S}$	$\mathcal{J}$	$\mathcal{S}$	$\mathcal{J}$
−0.598532		−0.606892	
	−0.596083		−0.604399
	−0.551438		−0.560157
−0.519167		−0.527075	
−0.475125		−0.482799	
	−0.420461		−0.428476
	−0.412278		−0.420440
−0.366859		−0.374389	
0.002564		−0.009322	
	0.004581		−0.005370
	0.136380		0.111551
0.154527		0.131881	
0.164060		0.145689	
	0.177475		0.161089
	0.334892		0.301960
0.339386		0.312243	
−378.654095[a]	−378.666190[a]	−379.100113[a]	−379.113753[a]

[a] E_{total}

Table 13. The π-MO eigenvalues and total energy, E_{total}, in a.u., of *o*-benzoquinodimethane ($\mathcal{S}$) and *p*-benzoquinodimethane ($\mathcal{T}$)

Standard geometry						Optimized geometry					
4-31G			MINI-4			4-31G			STO-3G		
$\mathcal{S}$	x^1	$\mathcal{T}$	$\mathcal{S}$	x^1	$\mathcal{T}$	$\mathcal{S}$	x^1	$\mathcal{T}$	$\mathcal{S}$	x^1	$\mathcal{T}$
		−0.509022			−0.601279			−0.510804			−0.466083
−0.508024			−0.600329			−0.508766			−0.464322		
	−0.489761				−0.582192		−0.484536			−0.438903	
		−0.405396			−0.508148			−0.409358			−0.361476
−0.388993			−0.492702			−0.392574			−0.344044		
−0.383475			−0.488711			−0.388363			−0.340926		
		−0.366905			−0.473427			−0.372965			−0.325567
		−0.264069			−0.377101			−0.274594			−0.217482
−0.260445			−0.371521			−0.268155			−0.213707		
0.069098			−0.002344			0.076043			0.186560		
		0.082833			0.010189			0.090340			0.193183
		0.173158			0.121204			0.181228			0.317247
0.196832			0.144618			0.202589			0.341374		
0.215930			0.155023			0.219362			0.345947		
		0.230028			0.175185			0.233369			0.369598
		0.371837			0.327538			0.374755			0.519419
0.383511			0.329172			0.384179			0.520821		
−307.092953[a]		−307.105335[a]	−306.432042[a]		−306.440292[a]	−307.093708[a]		−307.106762[a]	−303.778184[a]		−303.786213[a]

[a] E_{total}

Table 11 confirms the rapid perturbational convergence of all PV–RR series to the correct limit in this case as well. By repeating the above *ab initio* calculations employing two different basis sets, i.e. 4-31G and MINI-4, we have verified (Table 13) that the MO energy patterns shown in Table 8 are invariant under this change of the basis set. By symmetry-constraint geometry optimizations (i.e. C_2 for the $\mathscr{S}$, and D_{2h} for the $\mathscr{T}$ isomer), allowing for non-planarity of the $\mathscr{S}$ isomer, we have also verified that the TEMO inversion located at $x^I \simeq -0.4$ a.u. is not due to the steric strain induced by coplanar CH_2 units. In the C_2 geometry, optimized for $\mathscr{S}$, the exocyclic C–C bonds deviate from planarity by an angle of about 3°, and the planes of the methylene units rotate conrotatorically a few degrees. The 4-31G calculations with these optimized geometries exhibit the same TEMO π-MO energy pattern as do all the other calculations presented above.

Thus, we conclude that in the case of benzoquinodimethanes, the averaged effect of the non-nearest-neighbor interactions represents the physical factors which compete with the molecular topology in conditioning the π-MO energy pattern.

(v) We return now to the STO-3G calculations of benzoquinones and benzoquinodimethanes $\mathscr{S}$ and $\mathscr{T}$ pairs. For all MO eigenvalues of the $\mathscr{S}$, $\varepsilon^{q^{\mathscr{S}}}$, and $\mathscr{T}$ isomer, $\varepsilon^{q^{\mathscr{T}}}$, one may calculate via the PV–RR procedure the corresponding power series in λ,

$$\varepsilon^{q^{\mathscr{X}}}(\lambda) = \sum_{j=0}^{\infty} \varepsilon_j^{q^{\mathscr{X}}} \lambda^j, \qquad \mathscr{X} = \mathscr{S} \text{ or } \mathscr{T}. \tag{19}$$

In practice, the summation of (19) terminates when the desired numerical accuracy of $\varepsilon^{q^{\mathscr{X}}}$ is achieved. Despite the fact that due to Eq. (14), only $\lambda = 1$ has physical significance, in what follows we will formally consider λ as a continuous variable, and, consequently, $\varepsilon^{q^{\mathscr{X}}}(\lambda)$ as a continuous function. Note that a TEMO inversion observed in the *ab initio* spectra implies that the qth π-MO eigenvalues of $\mathscr{S}$ and $\mathscr{T}$ have crossed in the interval $\lambda \in [0, 1]$ passing from the topologically determined eigenvalues, $\varepsilon_0^{q^{\mathscr{X}}}$, to the *ab initio* ones, $\varepsilon^{q^{\mathscr{X}}}$. Such a crossing implies that $\varepsilon^{q^{\mathscr{T}}}(\lambda) - \varepsilon^{q^{\mathscr{S}}}(\lambda) = \varepsilon^{q}(\lambda) = 0$. For the purpose of the present paper, we restrict our considerations only to positive zeros, λ_i, of $\varepsilon^q(\lambda)$, which reflect the tendency of the MO eigenvalues considered to invert. Certainly, from these positive roots, only those have significance which are smaller than the radius of convergence. Let us call λ_{crit} the smallest positive root of $\varepsilon^q(\lambda) = 0$ which also satisfies the condition

$$\lambda_{\text{crit}} < \min\{r^{q^{\mathscr{S}}}, r^{q^{\mathscr{T}}}\}; \tag{20}$$

here, $r^{q^{\mathscr{X}}}$ denotes the radius of convergence corresponding to the power series (19). Evidently, $\lambda_{\text{crit}} > 1$ indicates the tendency of the orbitals in question to invert, but the inversion cannot be realized. For the same reason, $0 < \lambda_{\text{crit}} \leq 1$ indicates an effective inversion in passing from topological to *ab initio* eigenvalues of the orbitals considered.

The power series (19) corresponding to the orbitals ($q=1$, Table 8) which invert the order in the case of benzoquinodimethanes are:

$$\varepsilon^{1\mathscr{S}} = -0.497043 + 0.344983(-1)\lambda - 0.313862(-3)\lambda^2 - 0.127939(-4)\lambda^3 - 0.665283(-6)\lambda^4, \quad (21)$$

$$\varepsilon^{1\mathscr{T}} = -0.495944 + 0.327288(-1)\lambda - 0.326310(-3)\lambda^2 - 0.200885(-4)\lambda^3 - 0.240839(-5)\lambda^4 - 0.452625(-6)\lambda^5, \quad (22)$$

and the inversion starts to occur at $\lambda_{\text{crit}} = 0.617264$.

In the case of benzoquinones, the corresponding series are ($q=5$, Table 6):

$$\varepsilon^{5\mathscr{S}} = 0.139249 + 0.602139(-2)\lambda + 0.131691(-3)\lambda^2 + 0.450504(-5)\lambda^3 - 0.946093(-7)\lambda^4, \quad (23)$$

$$\varepsilon^{5\mathscr{T}} = 0.140496 + 0.460968(-2)\lambda + 0.337030(-4)\lambda^2 - 0.207554(-6)\lambda^3, \quad (24)$$

and the inversion starts to occur at $\lambda_{\text{crit}} = 0.833244$.

Note that $\lambda_{\text{crit}} < 1$ by a comfortable margin in the case of benzoquinodimethanes, and lies much closer to unity in the case of the benzoquinones. Further, we can correlate our results for the benzoquinones in the various basis sets by observing that the changes in the relative balance of tight-binding vs. non-nearest-neighbor interactions will tend to shift the actual value of λ_{crit} to values $\lambda_{\text{crit}} > 1$ more readily when this parameter lies closer to unity. By comparing λ_{crit} corresponding to (21), (22) and (23), (24) (consider the corresponding slopes too!), one sees that it is not surprising that the TEMO inversions observed in the STO-3G calculations of benzoquinones vanish on changing the basis set, but they persist for the same pair of MO's under this change in the case of benzoquinodimethanes.

(vi) The calculations reported herein and elsewhere [6, 7, 19] reveal that the TEMO patterns of the topological Hamiltonians associated with different $\mathscr{S}$ and $\mathscr{T}$ pairs exhibit a wide variety of system-dependent behavior (e.g. no inversions, inversions only in the second step, inversions in both steps, etc.) in passing to the patterns of the corresponding HF SCF Hamiltonians via the perturbational steps (17) and (18). As demonstrated above, the present formalism is able to detect and identify these effects, but the explanation of their diverse behavior remains an open question. For example, chemical intuition anticipates that the benzoquinodimethane isomers should undergo a smaller number of TEMO inversions than the benzoquinone isomers. Nevertheless, the actual SCF calculations (cf. Tables 5 and 12, and 8 and 13) reveal that, in fact, the reverse is true; thus, the benzoquinodimethanes display an inversion of the lowest-lying orbitals while the benzoquinones are in complete accord with the TEMO theorem (7). These

results suggest that perhaps such behavior might be traced, via an extension of the PV-RR analysis, to the competition between different responses of the unperturbed systems to different strengths of the perturbations *per se*; but this requires further investigation.

(vii) Our perturbational approach is rendered feasible by a combination of two essential factors: (1) The TEMO theorem which plays a central role in the partitioning of the matrices and the interpretation of the results since it leads to an unambiguous choice of the zero-order Hamiltonian matrix with a corresponding well-defined topologieal eigenvalue pattern; and (2) the unique flexibility of PV-RR (see Appendix A for further details) as an analytical tool which permits the accurate calculation of all MO eigenvalue perturbation corrections to arbitrarily high order for any topologically and/or physically conditioned partitioning of the SCF Hamiltonian matrices, thus enabling one to monitor in a continuous manner the passage from topology to physics.

6. Conclusions

We have shown analytically that the MO pattern of topologically related molecules exhibits a general interlacing rule, i.e. the TEMO theorem (7). Three models of selected topologically related pairs of isomers, which have chemical relevance, are discussed in detail and illustrated with experimental results. In addition, non-empirical SCF MO calculations have been performed for several representative pairs of topological isomers. In view of the great diversity in the nature of the constituent atoms and the large variation in the geometries of the molecules treated, we consider the remarkable agreement between the calculations reported herein, as well as of previous results [3-7], with the predicted TEMO behavior as evidence of the dominant influence of topology on the electronic structure of molecules.

Application of the PV-RR procedure in conjunction with the non-empirical SCF MO calculations has permitted us to dissect in quantitative detail the perturbing effect of certain apparently small but significant physical factors on the TEMO pattern. We conclude that the PV-RR analysis, coupled with critical λ considerations, yields insight which would be obscured by straightforward numerical approaches. In this connection, it should be noted that the unique flexibility of the PV-RR procedure as an analytical tool arises from the possibility of partitioning the Hamiltonian matrix in accordance with physical rather than mathematical requirements. In conventional RS perturbation theory [26] the reverse is often true, because one requires the complete spectrum of the exact zero-order eigenfunctions of the operator underlying the zero-order Hamiltonian matrix.

To our knowledge, our approach links, for the first time, the topological features of molecules to some of their physical properties in a rigorous and quantitative manner.

Acknowledgment We thank Dr. B. S. Sudhindra for adapting the program which he developed for PV-RR calculations. Thanks are also due to Dr. H. Kupka for critically reading the manuscript.

Appendix A. Some technical details of the PV–RR formalism

The appropriate substitution of (12) and (13) into (11) yields the hierarchy of coupled PV-RR equations,

$$\sum_{k=0}^{j} (\tilde{H}_k \tilde{C}_{j-k} - \tilde{C}_k E_{j-k}) = 0, \qquad j = 0, 1, \ldots, \tag{A.1a}$$

$$\sum_{k=0}^{j} \tilde{C}_k^{\dagger} \tilde{C}_{j-k} = I\delta_{0j}, \qquad j = 0, 1, \ldots. \tag{A.1b}$$

The initial step consists of solving the zero-order equations,

$$\tilde{H}_0 \tilde{C}_0 - \tilde{C}_0 E_0 = 0, \tag{A.2a}$$

$$\tilde{C}_0^{\dagger} \tilde{C}_0 = I, \tag{A.2b}$$

for E_0 and $\tilde{C}_0$ by standard diagonalization where the elements ε_0^s of E_0 are the roots of the secular determinant,

$$|\tilde{H}_0 - \varepsilon_0 I| = 0. \tag{A.2c}$$

Note that in the present formalism, it is required that the ε_0^s form a nondegenerate spectrum; for the topological isomers studied, we have found this condition to be fulfilled for the zero-order Hamiltonians $\tilde{H}_0$ and $\tilde{H}(1)$ of (17) and (18), respectively, when these matrices are constructed as shown in Appendix B.

The $E_j, j = 1, 2, \ldots$, are now determined successively by three independent methods [8b] which afford a valuable check on the internal consistency and accuracy of the calculations. The first method, which we term the basic PV-RR formalism, follows from premultiplying (A.1a) by $\tilde{C}_0^{\dagger}$, and also yields as output the $\tilde{C}_j, j = 1, 2, \ldots$; the second method exploits the generalized PV-RR Hellmann-Feynman theorem; and the third the generalized PV-RR remainder theorem. In all cases, the results are expressed compactly by introducing a number of auxiliary matrices which enable the recursive *concurrent* calculation of the RS series of all m orbitals in one computer run. Thus, one obtains via the basic formalism

$$E_j = [P_j]^{\mathrm{diag}}, \qquad j = 1, 2, \ldots, \tag{A.3a}$$

$$\tilde{C}_j = \tilde{C}_0 Q_j, \qquad j = 1, 2, \ldots, \tag{A.3b}$$

via the Hellmann-Feynman theorem,

$$E_j = [F_j]^{\mathrm{diag}}, \qquad j = 1, 2, \ldots, \tag{A.4}$$

and via the remainder theorem,

$$E_{2j} = [R_{2j}]^{\mathrm{diag}}, \qquad E_{2j+1} = [R_{2j+1}]^{\mathrm{diag}}, \qquad j = 1, 2, \ldots, \tag{A5a, b}$$

where $[X]^{\mathrm{diag}}$ denotes the diagonal matrix constructed from the diagonal elements of an arbitrary square matrix X. The various auxiliary matrices are defined as

$$P_j \equiv \tilde{C}_0^{\dagger} \sum_{k=1}^{j} [\tilde{H}_k \tilde{C}_{j-k} - (1 - \delta_{kj}) \tilde{C}_k E_{j-k}], \qquad j = 1, 2, \ldots, \tag{A.6}$$

$$Q_j^{tu} \equiv (\varepsilon_0^u - \varepsilon_0^t)^{-1} P_j^{tu}, \qquad t \neq u, \qquad j = 1, 2, \ldots, \tag{A.7a}$$

$$Q_j^{tt} \equiv -\frac{1}{2} \left[\sum_{k=1}^{j-1} \tilde{C}_k^{\dagger} \tilde{C}_{j-k} \right]^{tt}, \qquad j = 1, 2, \ldots, \tag{A.7b}$$

$$F_j \equiv j^{-1} \sum_{k=0}^{j-1} \sum_{i=0}^{j-k-1} (i+1) \tilde{C}_k^{\dagger} \tilde{H}_{i+1} \tilde{C}_{j-k-i-1}, \qquad j = 1, 2, \ldots, \tag{A.8}$$

$$R_{2j} \equiv \sum_{i=1}^{j} \sum_{k=j-i}^{j-1} \tilde{C}_k^{\dagger}(\tilde{H}_i \tilde{C}_{2j-i-k} - \tilde{C}_{2j-i-k} E_i) + \sum_{i=j+1}^{2j} \sum_{k=0}^{2j-i} \tilde{C}_k^{\dagger} \tilde{H}_i \tilde{C}_{2j-i-k}, \qquad j = 1, 2, \ldots, \tag{A.9a}$$

$$R_{2j+1} \equiv \sum_{i=1}^{j} \sum_{k=j+1-i}^{j} \tilde{C}_k^{\dagger}(\tilde{H}_i \tilde{C}_{2j+1-i-k} - \tilde{C}_{2j+1-i-k} E_i) + \sum_{i=j+1}^{2j+1} \sum_{k=0}^{2j+1-i} \tilde{C}_k^{\dagger} \tilde{H}_i \tilde{C}_{2j+1-i-k}, \qquad j = 1, 2, \ldots; \tag{A.9b}$$

here, the off-diagonal and diagonal elements of the Q_j matrix are given, respectively, by $Q_j^{[u]}$, (A.7a), and $Q_j^{[l]}$, (A.7b), where the latter impose the orthonormality conditions of (A.1b). Note that both the off-diagonal and diagonal elements of the P_j and Q_j matrices are required, but only the diagonal elements of the F_j, R_{2j}, and R_{2j+1} matrices. Note also from the structure of the various auxiliary matrices that for $j = 1, 2, \ldots$, calculation of the E_j from P_j and F_j requires a knowledge of the lower-order $\tilde{C}_k$ and E_k through $k = j-1$ while calculation of the E_{2j} and E_{2j+1} from R_{2j} and R_{2j+1} requires only a knowledge of the lower-order $\tilde{C}_k$ and E_k through $k = j$. The PV-RR calculations of (A.3)-(A.9) assume a natural cyclic structure which may be summarized as follows: After the nth cycle is completed, the $\tilde{C}_j$ and E_j will have been computed (the latter by three independent methods) for $j = 1, 2, \ldots, n$, and, in addition, the E_j, $j = n+1, n+2, \ldots, 2n+1$, will have been determined via the remainder theorem, (A.5).

For completeness, in (A.6), (A.8), and (A.9), we have introduced the generalized auxiliary matrices corresponding to the infinite-order $\tilde{H}$ of (12). This formulation is useful because in some applications, one needs to work with $\tilde{H}$ of higher order than the linearly perturbed cases of (17) and (18) used in the present analysis. Specifically, these generalized auxiliary matrices are brought into the appropriate form for linearly perturbed $\tilde{H}$ [8c] as follows: In (A.6), the summation over terms in $\tilde{H}_k$ reduces to the single term in $k = 1$, $\tilde{C}_0^{\dagger} \tilde{H}_1 \tilde{C}_{j-1}$, while the summation over the terms in E_{j-k} is unaffected; in (A.8), the summation over i reduces to the single term in $i = 0$; and in (A.9a) and (A.9b), the first double summation over terms in $\tilde{H}_i$ reduces, respectively, to the single term in $i = 1$, $\tilde{C}_{j-1}^{\dagger} \tilde{H}_1 \tilde{C}_j$ and $\tilde{C}_j^{\dagger} \tilde{H}_1 \tilde{C}_j$, the remainder of this double summation over terms in E_i is unaffected, and the second double summation over terms in $\tilde{H}_i$, $i = j+1, j+2, \ldots$, vanishes. Reduction of (A.6), (A.8), and (A.9) to the appropriate form for quadratically, cubically, etc., perturbed $\tilde{H}$ proceeds analogously. The remainder of the PV-RR formalism goes through unchanged; thus, the above remarks concerning the cyclic structure of the calculations, the remainder theorem, etc., remain valid regardless of the degree of truncation of the λ-expansion of $\tilde{H}$.

We complete this Appendix by summarizing those aspects of the PV-RR formalism which render it well suited for the perturbational analysis of the physical origins of TEMO inversions.

The PV-RR procedure is, as the name implies, a method for obtaining the solutions of the variational finite-dimensioned matrix eigenvalue equation (11a) (or, more generally, (10)) in the form of perturbational (Taylor) expansions in powers of λ about a corresponding zero-order matrix eigenvalue problem (A.2); all higher-order perturbational corrections are given *exactly* in terms of the PV-RR zero-order solutions E_0 and $\tilde{C}_0$ (cf. Eqs. (A.3)-(A.9) of Appendix A), which span the finite-dimensional Hilbert subspace of the original problem (11a). Since these zero-order solutions can always be obtained regardless of the choice of the unperturbed (Hermitian) $\tilde{H}_0$, for dummy λ we can partition $\tilde{H}$ into $\tilde{H}_0$ and a perturbing remainder $\Delta\tilde{H} = \tilde{H} - \tilde{H}_0$, or equivalently, change the origin of λ, in any manner we please; further, for the same reasons, we are then at liberty to decompose $\Delta\tilde{H}$ into any number of successive perturbational steps by shifting the λ-origin from $\tilde{H}_0$ to $\tilde{H}(1)$, $\tilde{H}(2)$, etc. in the general manner called for by (14), and, in particular, in accordance with the physically conditioned requirements of (17) and (18); this degree of freedom in the selection of the PV-RR λ-origin is crucial to the analysis of TEMO. Finally, the invariant structure of the PV-RR perturbational corrections, (A.3)-(A.5), enables the accurate recursive calculation of all PV-RR series to very high perturbational order; in this connection, the convergence properties of these series is subject to our rigorous control via (15) and (16).

Appendix B. Explicit construction of PV–RR TEMO matrices

The explicit construction of the matrices used in the PV–RR study of TEMO inversions is summarized below. Let $[Y]^{pq}$, $p, q = 1, 2, \ldots, m$, denote the elements of an arbitrary $m \times m$ matrix Y; in the present case (cf. Eqs. (17) and (18)), $Y = \tilde{H}_0, \tilde{H}_1(1), \tilde{H}_1(2), \tilde{H}$, where $\tilde{H}$ is that block of the SCF matrix which corresponds to the π-electron MO. Denote by $r \in \mathscr{S}$ or $r \in \mathscr{T}$ the diagonal elements of the matrix corresponding, respectively, to the $\mathscr{S}$ or $\mathscr{T}$ isomers, by $st \in \mathscr{S}$ or $st \in \mathscr{T}$ the off-diagonal elements corresponding to the tight-binding interactions in $\mathscr{S}$ or $\mathscr{T}$, and by $uv \in \mathscr{S}$ or $uv \in \mathscr{T}$ the off-diagonal non-tight-binding elements in $\mathscr{S}$ or $\mathscr{T}$. Evidently, m gives the number of atoms participating in the π-system; further, let k represent the number of bonds among these atoms. Then, the following relations are used:

$$[\tilde{H}_0]^{rr} = \frac{1}{2m}\left\{\sum_{r\in\mathscr{S}} [\tilde{H}]^{rr} + \sum_{r\in\mathscr{T}} [\tilde{H}]^{rr}\right\}, \tag{B.1}$$

$$[\tilde{H}_0]^{st} = \frac{1}{2k}\left\{\sum_{st\in\mathscr{S}} [\tilde{H}]^{st} + \sum_{st\in\mathscr{T}} [\tilde{H}]^{st}\right\}, \tag{B.2}$$

$$[\tilde{H}_0]^{uv} = 0, \qquad uv \in \mathscr{S}, \mathscr{T}. \tag{B.3}$$

Eqs. (B.1)-(B.3) impose only the topological constraints on the MO eigenvalue spectra. The effect of the SCF tight-binding interactions is then introduced via

$$[\tilde{H}_1(1)]^{rr} = [\tilde{H}]^{rr} - [\tilde{H}_0]^{rr}, \qquad r \in \mathscr{S}, \mathscr{T}, \tag{B.4}$$

$$[\tilde{H}_1(1)]^{st} = [\tilde{H}]^{st} - [\tilde{H}_0]^{st}, \qquad st \in \mathscr{S}, \mathscr{T}, \tag{B.5}$$

$$[\tilde{H}_1(1)]^{uv} = 0, \qquad uv \in \mathscr{S}, \mathscr{T}. \tag{B.6}$$

Note that, of course $[\tilde{H}]^{rr\in\mathscr{S}} \neq [\tilde{H}]^{rr\in\mathscr{T}}$ and $[\tilde{H}]^{st\in\mathscr{S}} \neq [\tilde{H}]^{st\in\mathscr{T}}$. Finally, the non-nearest-neighbor interactions are taken into account by writing

$$[\tilde{H}_1(2)]^{rr} = [\tilde{H}_1(2)]^{st} = 0, \qquad r \in \mathscr{S}, \mathscr{T}, \qquad st \in \mathscr{S}, \mathscr{T}, \tag{B.7}$$

$$[\tilde{H}_1(2)]^{uv} = [\tilde{H}]^{uv}, \quad uv \in \mathscr{S}, \mathscr{T}. \tag{B.8}$$

Clearly, the various matrices are constructed so that for the $\mathscr{S}$ and $\mathscr{T}$ isomers, we have

$$\tilde{H}_0 + \tilde{H}_1(1) + \tilde{H}_1(2) \equiv \tilde{H}. \tag{B.9}$$

It follows that the perturbational corrections introduced via (17) and (18) to the eigenvalues of $\tilde{H}_0$ must reproduce the SCF MO eigenvalues, provided that the associated PV–RR series converge; in all cases investigated, it has been verified both numerically and theoretically that the above partitioning scheme induces perturbational convergence.

References

1. Prelog, V.: J. Mol. Catalysis **1**, 159 (1975/76)
2. Polansky, O. E. in: Application of graph theory in chemistry, Chap. 1, Tyutyulkov, N., Bonchev, D., eds. Sofia: Science and Arts Publisher, in press
3. Polansky, O. E.: J. Mol. Struct. **113**, 281 (1984)
4. Polansky, O. E., Zander, M.: J. Mol. Struct. **84**, 361 (1982)
5. Polansky, O. E., Zander, M., Motoc, I.: Z. Naturforsch. **38a**, 196 (1983); Fabian, W., Motoc, I., Polansky, O. E.: Z. Naturforsch. **38a**, 916 (1983)
6. Motoc, I., Silverman, J. N., Polansky, O. E.: Phys. Rev. **A28**, 3673 (1983)
7. Motoc, I., Silverman, J. N., Polansky, O. E.: Chem. Phys. Lett. **103**, 285 (1984)
8. (a) Silverman, J. N., Sobouti, Y.: Astron. Astrophys. **62**, 355 (1978); (b) Silverman, J. N.: J. Phys. **A 16**, 3471 (1983); (c) Silverman, J. N., Pakiari, A. H.: in preparation
9. (a) Graovac, A., Gutman, I., Polansky, O. E.: Mh. Chem. **115**, 1 (1984); (b) Graovac, A., Polansky, O. E.: Croat. Chim. Acta, in press

10. Ruedenberg, K.: J. Chem. Phys. **22** 1878 (1954); **29**, 1232 (1958); **34**, 1884 (1961)
11. Weltin, E., Weber, J. P., Heilbronner, E.: Theoret. Chim. Acta (Berl.) **2**, 114 (1964), and references cited therein
12. Graovac, A., Gutman, I., Trinajstic, N.: Topological approach to the chemistry of conjugated molecules, Lecture notes in chemistry, Vol. **4**, Berlin: Springer Verlag 1977
13. Pancir, J.: Coll. Czech. Chem. Comm. **45**, 2452, 2463 (1980)
14. Silverman, J. N.: Phys. Rev. **A 23**, 441 (1981), and references cited therein
15. Two independent proofs of (7) are offered: Graovac, A., Gutman, I., Polansky, O. E.: in preparation; Gutman, I., Graovac, A., Polansky, O. E.: in preparation
16. Potzinger, P., Landers, A.: unpublished results
17. Schmidt, W.: J. Chem. Phys. **66**, 828 (1977)
18. Galasso, V., Colonna, F. P., Distefano, G.: J. Electron. Spectrosc. Relat. Phenom. **10**, 227 (1977)
19. Motoc, I., Silverman, J. N., Polansky, O. E.: Phys. Rev. **A** to be submitted
20. Dupuis, M., Rys, J., King, H. F.: QCPE Program Nos. 401/403, Indiana Univ., Bloomington
21. (a) Hehre, W. J., Stewart, R. F., Pople, J. A.: J. Chem. Phys. **51**, 2657 (1969); (b) Dunning Jr., T. H., Hay, P. J., in: Modern theoretical chemistry. Vol. 3. Methods of electronic structure theory, p. 1, Schaefer III, H. F. ed. New York: Plenum Press 1977; (c) Ditchfield, R., Hehre, W. J., Pople, J. A.: J. Chem. Phys. **54**, 724 (1971); (d) Tatewaki, H., Huzinaga, S.: J. Comp. Chem. **1**, 205 (1980)
22. Löwdin, P. O.: J. Chem. Phys. **18**, 365 (1950)
23. Sudhindra, B. S., Olbrich, G., Silverman, J. N.: in preparation
24. Silverman, J. N.: Phys. Rev. A **28**, 498 (1983), and references cited therein
25. Tables of interatomic distances and configuration in molecules and ions. London: The Chemical Society, 1958
26. See, for example, Hirschfelder, J. O., Brown, W. B., Epstein, S. T.: Adv. Quantum Chem. **1**, 255 (1964)

Received April 24, 1984